26th December 2004 Great Sumatra-Andaman Earthquake: co-seismic and post-seismic motions in northern Sumatra

by Jean-Claude Sibuet[a], Claude Rangin[b], Xavier Le Pichon[b], Satish Singh[c], Antonio Cattaneo[a], David Graindorge[d], Frauke Klingelhoefer[a], Jing-Yi Lin[a], Jacques Malod[d], Tanguy Maury[a], Jean-Luc Schneider[e], Nabil Sultan[a], Marie Umber[a], Haruka Yamaguchi[f] and the "Sumatra aftershocks" team

[a]Ifremer Centre de Brest, B.P. 70, 29280 Plouzané cedex, France

[b]Collège de France, Chaire de Géodynamique and CNRS CEREGE, Europôle de l'Arbois, BP 80, 13545 Aix en Provence, France

[c]Institut de Physique du Globe de Paris, 4 Place Jussieu, Tour 14-15, 5th Floor, 75252 Paris cedex 05, France

[d]Institut Universitaire Européen de la Mer, Place Nicolas Copernic, 29280 Plouzané, France

[e]Université Bordeaux 1, Observatoire Aquitain des Sciences de l'Univers, Département de Géologie et Océanographie, Avenue des Facultés, 33405 Talence cedex, France

[f]Institute for Research on Earth's Evolution, Japan Agency for Marine-Earth Science and Technology, Natsushima-cho 2-15, Yokosuka, 237-0061, Japan

"Sumatra aftershocks" team: J.-C. Sibuet, S. Singh, R. Apprioual, N.C. Aryanto, J. Begot, A. Cattaneo, A. Chauhan, R. Creach, J. Crozon, A. Domzig, N. Falleau, D. Graindorge, F. Harmegnies, Y. Haryadi, F. Klingelhoefer, S.K. Kolloru, J.-Y. Landuré, C. Le Lann, J. Malod, A. Normand, G. Oggian, C. Rangin, D. Restuning Galih, J.-L. Schneider, N. Sultan, M. Taufik, M. Umber and H. Yamaguchi.

Submitted to Earth and Planetary Science Letters, 31 August 2006

Revised, 1 March 2007

Corresponding author: Jean-Claude Sibuet, Ifremer Centre de Brest, B.P. 70, 29280 Plouzané cedex, France, jcsibuet@ifremer.fr, Ph. (33) 2 98 22 4233, mobile (33) 6 62 12 45 20

Abstract

Trench-parallel thrust faults verging both landward and seaward were mapped in the portion of wedge located between northern Sumatra and the Indian-Indonesian boundary. The spatial aftershocks distribution of the 26th December 2004 earthquake shows that the post-seismic motion is partitioned along two splay faults, the Lower and Median Splay Faults, the latter being right-laterally offset by a N-S lower plate fracture zone located along the 92.6°N meridian. Between February 2005 and August 2005, the aftershock activity shifted from southeast of this fracture zone to northwest of it, suggesting that the lower plate left-lateral motion along the fracture zone may have induced a shift of the upper plate post-seismic activity along the Median Splay Fault. Based on swath bathymetric and 3.5 kHz data, co-seismic deformations were weak

close to the trench. Joint seismic-geodetic determination of slip distribution and time arrivals and heights of tsunami waves suggest that the co-seismic slip was maximum along a portion of the Upper Splay fault located north of the Tuba Ridge. As the Upper Splay Fault is steeper than the slab, the vertical motion of the adjacent Outer Arc and overlying water is much larger compared to the one resulting from slip on the megathrust alone, increasing tsunamogenic effects.

Keywords: 2004 Sumatra-Andaman earthquake; aftershocks; co-seismic rupture; active splay faults

1. Introduction

The 26th December 2004 *Mw* 9.2 great Sumatra-Andaman earthquake ruptured the Sumatra and Sunda subduction zones over a length of 1300 km and generated the most deadly tsunami in the historic record. Teleseismically well-recorded earthquakes occurring in this region during the 1918–2005 period were relocated by Engdahl et al. {, 2007 #514}. Prior to the 2004 earthquake the seismicity occurred downdip along the interplate zone at depths greater than 35 km, with a clear near absence of seismicity trenchward {Engdahl, 2007 #514; Lay, 2005 #510} (Fig. 1). The co-seismic slip distribution of the Sumatra-Andaman earthquake has been estimated from seismic waves {Ammon, 2005 #492; Lay, 2005 #510}, static offsets {Banerjee, 2005 #518; Subarya, 2006 #476; Vigny, 2005 #491}, and joint seismic-geodetic data {Chlieh, 2007 #515}. Most of the co-seismic slip occurred trenchward of prior seismicity and was close to its maximum value of ~20 m {Ammon, #492; Subarya, 2006, #476} offshore NW Sumatra where the tsunami devastated the coast along ~300 km, causing 170,000 of the 230,000 tsunami deaths. Concerning the aftershock activity, most of it is located trenchward at depths less than 35 km, filling in areas with an absence of previous seismicity {Engdahl, 2007 #514} (Fig. 1b). However, many aftershocks are also observed between 35 and 75 km, in particular in the northern Sumatra area (Fig. 1b). Therefore, the rupture of the northern Sumatra area seems to present specific characteristics during the northward propagation of the 2004 earthquake.

To understand why the co-seismic slip and tsunami amplitudes were so high in this region, we performed the "Sumatra Aftershocks" cruise (R/V Marion Dufresne, Jakarta, July 15 - Colombo, August 9, 2005) in order to establish the geodynamical context of the 2004 earthquake and to record the aftershock activity. We selected an area which covers the whole subduction system from the Wharton Basin to northeast of the Sumatra Fault and located between northern Sumatra and the Indonesia/India water limit. Twenty ocean bottom seismometers (OBS) were deployed and recorded the local seismicity during 12 days. During the recording period, a 370x75 km stripe was fully surveyed (Fig. 2) with a Seafalcon 11 MBES swath-bathymetric system (the bathymetric grid will be available at http://www.ifremer.fr).

2. Geodynamic context

Offshore northern Sumatra, the motion is close to the Australia/Sunda motion {Delescluse, 2007 #508}, that is about 47 mm/yr to N004° {Socquet, 2006 #512}. The focal mechanism of the 26th December 2004 great Sumatra-Andaman earthquake shows

that partitioning due to the obliquity of the subduction is complete because the co-seismic motion is perpendicular to the trench, along N039° {Lay, 2005 #510}. This gives 38.5 mm/yr for the motion perpendicular to the trench and 29.5 mm/yr to N309° for the right-lateral motion. The motion along the right-lateral Sumatra Fault is estimated to be about 25 mm/yr in northernmost Sumatra {Sieh, 2000 #511}. This suggests that at most 5 mm/yr are absorbed by dextral deformation within the wedge.

Northwest of Sumatra Island, the Sumatra Fault system extends in a ~50-km wide dextral shear band, which continues at sea in the northern part of the bathymetric survey (Fig. 2). Aligned volcanoes suggest that the northern branch of the system, which is named the Sumatra Fault by Sieh and Natawidjaja {, 2000 #511} is the most recent active segment as summarized by Curray {, 2005 #499}. In the Aceh forearc basin, fossil linear faults parallel to the Sumatra Fault, sometimes showing a compressive component, were identified in its southern portion {Izart, 1994 #498}. Along the northeastern slope of the Outer Arc, southwest of the Aceh Basin, a festoon of discontinuous and discrete strike-slip faults was observed and corresponds to the location of the West Andaman Fault (Fig. 3). To the northwest, this dextrally wrenched system merges with the Sumatra Fault system that then proceeds toward the Andaman Sea. To the southeast, its connection with the Mentawai Fault located north of Simeulue Island (e.g. {Izart, 1994 #498}) or with a former plate boundary located south of Simeulue Island {Curray, 2005 #499} is still unclear. Even if two strike-slip aftershocks occurred close to the West Andaman Fault in the days following the 26 December event {Singh, 2005 #500} and if the two Sumatra and West Andaman fault systems are geologically active systems, they were not active during the 2004 earthquake. Consequently, the stress is still accumulating along the two Sumatra and West Andaman fault systems and one of the two systems at least may break in the future.

The wedge, located between the tectonic front and the broad 40-50 km wide Outer Arc adjacent to the Aceh forearc basin, is 130-km wide (Fig. 2) {Fisher, 2007 #503}. Most of the wedge is at a mean depth of 1.5 km and consists of a series of sigmoidal ridges and troughs that formed several piggy-back basins (Fig. 3). We assume that the sigmoidal shape of these features is the signature of distributed dextral wrenching within the wedge. Most of the piggy-back basins are bordered by reverse faults and thrusts with double vergency as shown in figures 4 and 5. About 30 of such thrust faults oriented N340° (parallel to the trench) with both seaward and landward vergences are imaged in the swath-bathymetric (Figs 2 and 3) and 3.5 kHz data. However, the post-seismic focal mechanisms related to the 2004 Sumatra earthquake only show sparse evidence for strike-slip motion within the wedge (Fig. 1d). Consequently, the structurally observed distributed dextral wrenching would have to be attributed to non-elastic interseismic motion.

Seismically active splay faults were suggested by the OBS recording of aftershocks {Araki, 2006 #496}. Some of the structures observed in the bathymetry and 3.5kHz data could mark the outcrops of splay faults. This is the case for the intense folding observed within the main piggy-back basin adjacent to the Outer Arc and associated recent deformations observed on 3.5 kHz data (Figs 4 and 5) that suggest the existence of a major thrust fault (Upper Splay Fault in Fig. 3) located beneath the Outer Arc and emerging S-W of it (Figs. 2 and 3).

In the frontal part of the wedge, where the water depth drops from 1 to 4 km in less than 20 km, a ROV exploration {Soh, 2005 #497} suggests that the most seaward active splay fault identified from the Japanese OBS data obtained southeast of our

survey {Araki, 2006 #496} may indeed emerge at the base of a giant anticline-like feature, characterized by a very steep southwest-facing wall with large erosional scarps. This wall is bounded at its base by a thrust fault (Major Thrust in Figs 2, 6 and 7a). Thus, the post-seismic deformation in the wedge may have been distributed along several splay faults throughout the wedge although we have no direct proofs that they were indeed active during the main shock. The four major splay faults identified from swath bathymetric and 3.5 kHz data are underlined in Figures 2, 3 and 6.

The explored segment of subduction zone is located above the diffuse India/Australia plate boundary identified between the Investigator Fracture Zone (98°E) and the Ninety East Ridge {Delescluse, 2007 #508}. The south to north velocity vector of the Australia plate with respect to the India plate determined in this stripe is parallel to the direction of the mapped oceanic fracture zones {Deplus, 1998 #493}. It progressively decreases westward across this diffuse boundary from about 1 cm/yr to zero {Delescluse, 2007 #508}. Earthquakes occurring within this stripe display N-S left-lateral strike-slip mechanisms (Harvard CMT focal mechanisms), which reactivate old fracture zones (e.g. Fig. 1d).

Seismic profiles do not show the emergence of the interplate fault plane {Moran, 2005 #494} and the Sunda Trench is not marked in the bathymetry (Figs 2 and 6). Seaward of the wedge, small-scale amplitude N-S oriented sedimentary ridges were identified on 3.5 kHz profiles (Figs 8 and 9) and correspond to the morphological expression of basement ridges of the underlying oceanic fracture zones. The subduction of these basement ridges indents and controls the morphology of the toe of the prism (Fig. 6). 3.5 kHz data clearly evidences N-S trending landward thrusting and folding of the frontal part of the wedge. Thus, we attribute the deformation of the frontal part of the wedge with re-entrants compatible with a dextrally wrenched tectonic front to the obliquity of the subducting N-S oriented lower plate basement features with the N340° sedimentary features and thrust faults of the wedge. In the study area, the signs of tectonic activity linked to the 2004 earthquake and located at the toe of the prism are weak and restricted to small-scale fault-related features and minor landslides {Henstock, 2006 #495} (Fig. 6). For example, a small 20-m deep depression (the ditch) that runs parallel with the base of a 12-km long scarp along the toe of the prism has been interpreted as an active feature {Moran, 2005 #494}. The excess pore pressure was measured in the sediments close to the landslide shown in Figure 7a. Sultan et al. {, 2007 submitted #520} have demonstrated that sediments were shaken at the time of the 2004 earthquake, generating an excess pore pressure at the origin of the most recent part of the landslide. As there is no evidence of large displacements at the frontal part of the wedge, it is an indirect proof that the co-seismic displacement has to be partitioned.

Several N-S oriented valleys not only cut across the whole wedge but apparently dextrally offset the N340° anticline and syncline features as well as thrust faults of the wedge, giving rise to sigmoidal dextral wrenched features (Figs. 3 and 7b). Some moderate size earthquakes with N-S right lateral strike-slip mechanisms have occurred during the interseismic and postseismic periods in the wedge (e.g. Engdahl, 2007). We suggest that this dextral deformation due to the motion of the upper plate with respect to the lower plate absorbs a small part of the shear partitioning. It is probably controlled by the topography of the N-S lower plate fracture zone ridges, along which sinistral shear motions were evidenced in the Wharton Basin (e.g. Engdahl, 2007) (Fig. 1c). Thus, the deformation of the sea floor would be partly related to the co- and post-seismic ruptures related to the 2004 large giant subduction earthquake (in particular the splay faults in

some of the piggy-back basins) and partly to the distributed dextral wrenching across the wedge, during the mostly non-elastic interseismic deformation.

3. Aftershock activity

As the aftershock activity decays rapidly with time, it was crucial to set up the OBS instruments as soon as possible. In order to image the whole subduction system with a better definition that the one obtained from land stations, 20 short-term OBSs were deployed with a mean 40-60 km distance between them from the Wharton Basin to north of the Sumatra Fault system (Fig. 10a). This distance between instruments is a compromise between the optimum distance to get the best depth determination of earthquakes originated from the slab (20-30 km) and the optimum distance to get tomographic images of the whole subduction system (70-100 km) including the marine portion of the Sumatra Fault system. This pool of OBSs consisted of 15 instruments based on the GEOMAR electronic system and 5 recently developed MicrOBSs {Auffret, 2004 #501}. Except for 15-minutes long noisy patches possibly due to ship noise, all OBSs recorded good hydrophone and three-component seismograms. We identified events recorded on at least 3 OBSs with a 1-D preliminary velocity law determined by inversion of seismic events, which is similar to the one used by Araki et al. {, 2006 #496}. In February-March 2005, Japanese deployed 17 short-term instruments during 19-22 days in a small area adjacent to our transect {Araki, 2006 #496} (Fig. 10a). As the 1-D velocity laws used in both experiments are similar, we have displayed in the same figure 1100 published hypocenters identified during the first 10 days of the Japanese experiment {Araki, 2006 #496} and 665 hypocenters identified during our experiment (Fig. 10a). The magnitude Md of earthquakes was determined by using the duration of seismic waves {Tsumara, 1967 #502}. As the depth determination of events located outside of the two OBS networks is poor, we only display a cross-section with events located within the two OBS networks (498 events from our OBS survey). Although earthquakes are not re-located for the moment with a 3-D velocity model and the dispersion of events projected on the cross-section (Fig 10b) is increased by the thrust fault bending in the area of the two OBS surveys, we can already emphasize a few important points:

- At 5.7°N, there is a marked transition in the distribution of aftershocks not caused by the distribution of seismometers and already noticed by Engdahl et al. {, 2007 #514} at 5.5°N (Figs 1b and 1d). This transition broadly corresponds to changes in the co-seismic slip distribution (e.g. {Chlieh, 2007 #515}) (Fig. 1a). South of 5.7°N, from the Sunda Trench to the Outer Arc, only small magnitude aftershocks developed (Fig 1b, 1d and 10), while further landward exists a dense cluster of larger magnitude thrust-fault aftershocks below the Aceh Basin and forearc, between depths of 30 and 55 km. North of 5.7°N the situation reverses. The large magnitude earthquakes occur closer to the trench axis, and there are few aftershocks farther than 75 km from the trench (Figs 1b and d).

- The dip angle of the slab increases from 10° between the Sunda Trench (0 km) and 120 km, to 10-12° between 120 and 170 km and to 15-20° beyond 170 km (Fig. 10b). From 0 to 170 km (i.e. beneath the accretionary wedge and Outer Arc), focal mechanisms are mostly in down-dip extension as shown by Araki et al. {, 2006 #496} and by teleseismic mechanisms (Figure 1d). However, the aftershock seismicity is weak between 120 and 170 km as also attested by the distribution of relocated seismicity {Engdahl, 2007 #514} between the dates of the Sumatra and Nias events, which shows

an absence of seismicity (except 3 earthquakes) in a 50-km wide band sitting astride the Upper Splay Fault (Fig. 1b). Beyond 170 km, the seismicity notably increases but seems to be located within plate interplate zone patches, ~30-km in size. Focal mechanisms become dip-slip type as shown by Araki et al. {, 2006 #496} and by the teleseismic mechanisms (Figure 1d), which has been interpreted as an ongoing post-seismic slip beneath the Aceh Basin and forearc {Araki, 2006 #496}.

- A cluster of 186 events was identified on the five deepest OBS stations, in the vicinity of the prism toe, complementing the Japanese data, which did not show such events in the first 40 km landward of the toe of the prism Fig. 10a). Before relocation, it is difficult to decipher if these events belong to the upper or lower plate, especially in the first 60 km from the Sunda Trench. However, events in the Wharton Basin belong to the oceanic crust, suggesting that the swarm of events located immediately N-E of the trench are related to lower plate post-seismic activity. As the Major Thrust, which might correspond to the outcrop of the main slab décollement, is not post-seismically active, the aftershock cluster of 186 events located on the Major Thrust is probably related to the left-lateral re-activation of a N-S trending fracture zone along the 93.2 °E meridian. The 3.5 kHz profile C (Figure 8) and swath bathymetric data (Figure 3) show this feature interpreted as a N-S oriented fold with a possible E-W compressive component. Another 3.5 kHz profile (Profile D in Figure 9) perpendicular to Profile C shows potential N-S left lateral strike slips in the area of the cluster of 186 events. However, as the 3.5 kHz penetration is only a few meters, seismic profiles are needed to fully resolve this question.

4. Splay faults

Within the upper plate, the distribution of aftershocks is concentrated in four areas:

1) In discrete patches localized in the oceanic crust of the Wharton Basin and beneath the frontal part of the accretionary wedge, along the 93.2°E fracture zone. Outside these patches, no aftershocks are recorded along the Major Thrust which is imaged in Fig. 9a and more generally S-W of the Lower Splay Fault emergence, between 0 and 60 km.

2) At 70 km, within the shallow part of the wedge, a first active splay fault is imaged (Fig. 10). Here, the precision in the depth determination of hypocenters is sufficient to discriminate between earthquakes belonging to the upper and lower plates. In plane view, aftershocks are located N-E of the trace of the Lower Splay Fault. The active portion of the Lower Splay Fault starts in the southeast at its intersection with the 93.6°E N-S valley (Figs 7b and 10). To the northwest, seismic events continues northwest of our survey until 5.7°N, following a northerly direction already underlined by a bathymetric trend in the Sandwell and Smith {, 1994 #121} map.

3) At 110 km, a second active N340° oriented splay fault (Median Splay Fault) is well imaged in cross-section and plane view (Fig. 10). The elongated cluster of seismic events begins south of the location of the Japanese network (94.4°E) and disappears at 5.7°N. We observed a shift in the post-seismic activity from S-E of the 93.6°E N-S valley (Figs 3 and 7b) at the time of the Japanese survey (February 2005) to N-W of this feature at the time of our survey (August 2005). This is not an artifact as both OBS pools recorded earthquakes well outside their networks. Even if the depth determination of seismic events is poor, some of them, located between 80 and 130 km, definitely belong to the underlying oceanic crust (Fig. 10b). The dense but diffuse seismic activity observed in the lower plate and spatially along the N-S 93.6°E feature, between 4.3°N

and 5.1°N, suggests that it is a re-activated portion of fracture zone which may act as an asperity for the northwestward jump of the aftershock activity along the Median Splay Fault between February and August 2005.

4) A hypothetical splay fault (Upper Splay Fault) that may rise from the slab break at 170 km and outcropping southwest of the Outer Arc has been suggested by Araki et al. {, 2006 #496}, though only a small number of upper plate events were recorded. This splay fault crops out where we have identified a major thrust fault on the basis of detailed bathymetric and 3.5 kHz data. Very recent active compressive features are shown on profiles A and B (Figs 4 and 5) located in Fig. 3. A popup feature and small-elongated tilted basins are observed within the piggy-back basin (Fig. 4). Further northwest in the same piggy-back basin, numerous seaward vergence thrust faults show signs of a recent tectonic activity (Fig. 5). Small thrust faults between 19H06 and 19H11 are testimonies of such a recent tectonic activity within a gently folded sub-basin. On the basis of a careful examination of all 3.5 kHz profiles, we suggest that the Upper Splay Fault is a very recent feature which is not post-seismically active.

5. Discussion and conclusion

From the careful examination of the aftershock activity, two post-seismic active splay faults were identified (Lower and Median Splay Faults in solid red lines) and two other splay faults are not post-seismically active (Major Thrust and Upper Splay Fault in dashed red lines, Fig. 10). Fig. 11c summarizes the distribution of post-seismic active features: dip-slip along the interplate zone beneath the Aceh basin and the deeper part of the forearc, and down dip extension beneath the accretionary wedge with the presence of two splay faults branching on the interplate zone. The two swarms of events located in the frontal part of the wedge and along the 93.6°E meridian suggest that this aftershock activity is linked to left-lateral strike slip motions along two fracture zones located at 93.2°E and 93.6°E longitude. Thus, the reactivation of two lower plate fracture zones triggered by the 2004 earthquake or due to the westward decrease of the velocity vector in the diffuse area of the Australia/India plate boundary influences the distribution of the aftershock activity within the accretionary wedge. By analogy, we suggest that the other N-S valleys identified in the swath bathymetric data (Figs 2, 3, 6 and 7) are associated with presently inactive underlying lower plate fracture zones.

Before the 2004 earthquake, the seismicity was restricted to northeast of the Upper Splay Fault and no teleseismic earthquakes were recorded below the accretionary wedge (Fig. 1a). Except if there is some aseismic creep within the accretionary wedge, the locked zone is located beneath the accretionary wedge, southwest of the Upper Splay Fault, which seems to be the landward boundary of the locked zone. Therefore, the Upper Splay Fault may play a significant role during the 2004 Sumatra earthquake.

The detailed joint seismic-geodetic determination {Chlieh, 2007 #515; Subarya, 2006 #476} shows that west of Andaman Islands the co-seismic slip occurred trenchward of the prior seismicity and as far as the trench (Fig. 1a). In contrast, between Simeulue Island (2.5°N) and south of Nicobar Island (6°N), the co-seismic slip curves overlap the prior seismicity and the co-seismic slip becomes null somewhere between the Median and Upper Splay Faults (Fig. 1a), suggesting that no co-seismic motion occurred along the Median Splay Fault, Lower Splay Fault and Major Thrust. Except if there was some aseismic creep within the accretionary prism, this observation explains why the deformation at the front of the wedge was so weak. If this is correct and knowing the uncertainty on the co-seismic slip values, the Upper Splay Fault branching

upward from the interplate zone might be a candidate for transferring the co-seismic slip from the interplate zone to the sea-bottom.

Plaker et al. {, 2006 #517} interviewed 110 eyewitnesses, who were situated along the west coast of Sumatra, and obtained information on wave arrival times, wave heights and wave periods. Tsunami flow depths of 5 to 12 m along the north coast and 7 to 20 m along the west coast cannot be explained by the 2.8 m vertical displacement estimate due to slip on the plate interface alone, assuming 20 m maximum horizontal slip, 8° fault dip, and dip-slip displacement {Plafker, 2006 #517}. Back tracing the recorded arrival times suggested that the source was located in the area of the Outer Arc, where Plafker et al. {, 2007 #516} reoccupied old bathymetric lines after the 2004 earthquake and found a recent uplift of more than 14 m. They show that a source model consisting primarily of co-seismic uplift along a splay fault about 80 km long, 60 degree dip, and 20 m slip that is superimposed on minor uplift (<3 m) due to up-dip slip on the megathrust explain the tsunami obervations. Banerjee et al. {, 2007 #521} also considered a hypothetical splay fault approximately coincident with the West Andaman Fault. When dip slip of 20 m is assigned to this splay fault and slip parameters are inverted, the remaining slip along the shallower portion of megathrust is only 2.9 m ± 2.1 m, which means that there is a kinematic discontinuity between the deeper and shallower slip on the megathrust in this area. Banerjee et al. {, 2007 #521} suggest that the disproportionate amount of aftershock activity deeper than 30 km imaged by Araki et al. {, 2006 #496} would reflect the much greater co-seismic slip having occurred along the deeper section of the megathrust. All these arguments suggest that the portion of the Upper Splay Fault located north of the Tuba Ridge ruptured during the 2004 Sumatra earthquake (Fig. 11b).

For large size earthquakes, the role of splay faults has been already evidenced. For example, during the 1964 Alaskan earthquake, a thrust displacement of 8 m along a splay fault was observed on the Patton Bay Fault in Montague Island {Plafker, 1972 #505}, suggesting that a substantial amount of deeper slip was transferred to the splay fault resulting in relatively little slip on the shallower megathrust. More recently, the co-seismic slip was modeled along an inferred splay fault for the 1946 Nankai earthquake {Cummins, 2000 #506}. In the Nankai subduction zone, the geometry of splay faults was imaged on deep seismic reflection profiles. One of the splay faults is branching upward from the interplate zone, beneath the forearc basin, and emerges seaward of the outer arc {Park, 2002 #504}, in a geological context similar to the one of our studied area. Similarly, for the 1958 earthquake on the Ecuador margin, co-seismic slip occurred along a megathrust splay fault located beneath the outer arc {Collot, 2004 #513}. The associated co-seismic uplift was interpreted as the cause of the triggered tsunami. Thus, splay faults must be taken into account to understand the behavior of megathrust earthquakes. Surface dips of splay faults are considerably larger (30° in the Nankai Trough) than the 10° dip angle of the slab at the prism toe, increasing the resulting vertical motion of the water column and giving rise to large tsunamis (Fig. 11b). We thus conclude that during the 2004 earthquake, the motion was transferred from the slab to the Upper Splay Fault and that it was the main factor controlling the large amplitude of the tsunami.

The N004° Australia/Sunda motion being partitioned between motions perpendicular to the trench along N039° (example of the 26th December 2004 earthquake) and right-lateral motions along the N309° direction, both the Sumatra Fault and the West Andaman Fault may rupture in the future as shown in Fig. 11d, giving rise

to destructive earthquakes associated with minor tsunamis as no significant vertical offsets are expected.

References

[1] E.R. Engdahl, A. Villaseñor, H.R. DeShon, C.H. Thurber, Teleseismic relocation and assessment of seismicity (1918–2005) in the region of the 2004 Mw 9.0 Sumatra-Andaman and 2005 Mw 8.6 Nias Island great earthquakes, Bull. Seism. Soc. Am. 97, doi:1785/0120050614(2007) 43-61.

[2] T. Lay, H. Kanamori, C.J. Ammon, M. Nettles, S.N. Ward, R.C. Aster, S.L. Beck, S.L. Bilek, M.R. Brudzinski, R. Butler, H.R. DeShon, G. Ekström, K. Satake, S. Sipkin, The great Sumatra-Andaman earthquake of 26 December 2004, Science 308(2005) 1127-1133.

[3] C.J. Ammon, C. Ji, H.K. Thio, D. Robinson, S. Ni, V. Hjorleifsdottir, H. Kanamori, T. Lay, S. Das, D. Helmberger, G. Ichinose, J. Polet, D. Wald, Rupture Process of the 2004 Sumatra-Andaman Earthquake, Science 308(2005) 1133-1139.

[4] P. Banerjee, F.F. Pollitz, R. Bürgmann, The size and duration of the Sumatra-Andaman Earthquake from far-field static offsets, Science 308(2005) 1769-1772.

[5] C. Subarya, M. Chlieh, L. Prawirodirdjo, J.-P. Avouac, Y. Bock, K. Sieh, A.J. Meltzner, D.H. Natawidjaja, R. McCaffrey, Plate-boundary deformation associated with the great Sumatra-Andaman earthquake, Nature 440, doi:10.1038/nature04522(2006) 46-51.

[6] C. Vigny, W.J.F. Simons, S. Abu, R. Bamphenyu, C. Satirapod, N. Choosakul, C. Subarya, A. Socquet, K. Omar, H.Z. Abidin, B.A.C. Ambrosius, Insight into the 2004 Sumatra–Andaman earthquake from GPS measurements in southeast Asia, Nature 436(2005) 201-206.

[7] M. Chlieh, J.-P. Avouac, V. Hjorleifsdottir, T.-R.A. Song, C. Ji, K. Sieh, A. Sladen, H. Hebert, L. Prawirodirdjo, Y. Bock, J. Galetzka, Coseismic slip and afterslip of the Great M_w 9.15 Sumatra-Andaman Earthquake of 2004, Bull. Seism. Soc. Am. 97, doi:1785/0120050631(2007) 152-173.

[8] M. Delescluse, N. Chamot-Rooke, Instantaneous deformation and kinematics of the India-Australia plate, Geophysical Journal International 168(2007) 818-842.

[9] A. Socquet, C. Vigny, N. Chamot-Rooke, W. Simons, C. Rangin, B. Ambrosius, India and Sunda plates motion and deformation along their boundary in Myanmar determined by GPS, Journal of Geophysical Research 111, B05406, doi:10.1029/2005JB003877(2006).

[10] K. Sieh, D.H. Natawidjaja, Neotectonics of the Sumatran Fault, Indonesia, Journal of Geophysical Research 105(2000) 28,295-228,326.

[11] J.R. Curray, Tectonics and history of the Andaman Sea region, Journal of Asian Earth Sciences 25(2005) 187-232.

[12] A. Izart, B. Mustafa Kemal, J.A. Malod, Seismic stratigraphy and subsidence evolution of the northwest Sumatra fore-arc basin, Marine Geology 12(1994) 109-124.

[13] S.C. Singh, Sumatra Aftershocks team, Sumatra earthquake research indicates why rupture popagated northward, EOS Transactions, American Geophysical Union 86(2005) 497-502.

[14] D. Fisher, D. Mosher, J.A. Austin, S.P.S. Gulick, T. Masterlark, K. Moran, Active deformation across the Sumatran forearc over the December 2004 M_w9.2 rupture, Geology 35(2007) 99-102, doi: 110.1130/G22993A.22991.

[15] E. Araki, M. Shinohara, K. Obana, T. Yamada, Y. Kaneda, T. Kanazawa, K. Suyehiro, Aftershock distribution of the 26 December 2004 Sumatra-Andaman earthquake from

ocean bottom seismographic observation, Earth, Planets and Space 58(2006) 113-119.
[16] W. Soh, Y.S. Djajadihardja, Y. Anantasena, K. Arai, E. Araki, S. Burhanuddin, T. Fujiwara, N.D. Hananto, K. Hirata, H. Kurnio, H. Machiyama, K.M. Badrul, C. Mueller, L. Seeber, K. Suyehiro, K. Wanatebe, Sea bottom shattered by the Sumatra-Andaman earthquake of 26 December 2004, EOS Transactions, American Geophysical Union, Supplement 86(2005) F8-9.
[17] C. Deplus, M. Diament, H. Hébert, B. Bertrand, S. Dominguez, J. Dubois, J. Malod, P. Patriat, B. Pontoise, J.-J. Sibilla, Direct evidence for active deformation in the eastern Indian Ocean plate, Geology 26(1998) 131-134.
[18] K. Moran, J.A. Austin, D.R. Tappin, Survey presents broad approach to tsunami studies, EOS Transactions, American Geophysical Union 86(2005) 430-432.
[19] T.J. Henstock, L. McNeill, D.R. Tappin, Seafloor morphology of the Sumatran subduction zone: Surface rupture during megathrust earthquakes?, Geology 34(2006) 485-488.
[20] S. Sultan, A. Cattaneo, J.-C. Sibuet, J.-L. Schneider, Sumatra Aftershocks team, Evidence from piezometer monitoring of in situ excess pore pressure and sediment deformation generated during the December 26, 2004 Great Sumatra-Andaman Earthquake, Journal of Geophysical Research(2007 submitted).
[21] Y. Auffret, P. Pelleau, F. Klingelhoefer, L. Geli, J. Crozon, J.-Y. Lin, J.-C. Sibuet, MicrOBS: A new generation of ocean bottom seismometer, first break 22(2004) 41-47.
[22] K. Tsumara, Determination of earthquake magnitude from duration of oscillation, Jishin (in Japanese) 2(1967) 30-40.
[23] D.T. Sandwell, W.H.F. Smith, New global marine gravity map/grid based on stacked ERS1, Geosat and Topex altimetry, EOS Transactions, American Geophysical Union 75 (16) Spring Meet. Suppl.(1994) 321.
[24] G. Plafker, L.S. Cluff, X. Lloyd, S.P. Nishenko, Y. Stuart, D. Syahrial, The cataclysmic 2004 tsunami on NW Sumatra - Preliminary evidence for a near-field secondary source along the Western Aceh Basin, Seism. Soc. Am., Annual meeting, San Francisco, CA, April, 2006, Abstract(2006).
[25] G. Plafker, S.N. Ward, S.P. Nishenko, L.S. Cluff, J. Coonrad, D. Syahrial, Evidence for a secondary tectonic source for the cataclysmic tsunami of 12/26/2004 on NW Sumatra, Seism. Soc. Am., Annual meeting, Kona, Hawaii, April 11-13, 2007, Abstract(2007).
[26] P. Banerjee, F.F. Pollitz, B. Nagarajan, R. Bürgmann, Coseismic slip distributions of the 26 December 2004 Sumatra–Andaman and 28 March 2005 Nias earthquakes from GPS static offsets, Bull. Seism. Soc. Am. 97, doi: 10.1785/0120050609(2007) 86-102.
[27] G. Plafker, Alaskan earthquake of 1964 and Chilean earthquake of 1960: implications for arc tectonics, Journal of Geophysical Research 77(1972) 901-923.
[28] P.R. Cummins, Y. Kaneda, Possible splay fault slip during the 1946 Nankai earthquake, Geophysical Research Letters 27(2000) 2725-2728.
[29] J.-O. Park, T. Tetsuro, S. Kodaira, P.R. Cummins, Y. Kaneda, Splay fault branching along the Nankai subduction zone, Science 297(2002) 1157-1160.
[30] J.-Y. Collot, B. Marcaillou, F. Sage, F. Michaud, W. Agudelo, P. Charvis, D. Graindorge, M.-A. Gutscher, G. Spence, Are rupture zone limits of great subduction earthquakes controlled by upper plate structures? Evidence from multichannel seismic reflection data acquired across the northern Ecuador-southwest Colombia margin, Journal of Geophysical Research 109, B11103, doi.1029/2004JB003060(2004).
[31] S.-K. Hsu, J.-C. Sibuet, Earthquake off Japan could generate strong tsunami, Eos 86(2005) 169-170.

Acknowledgments: We thank the Presidents of Ifremer and Institute Paul-Emile Victor (IPEV) for their constant supports and encouragements to achieve on a short notice the "Sumatra Aftershocks" cruise onboard the R/V Marion Dufresne. We thank Yvon Balut (IPEV), Pierre Cochonat (Ifremer), John Ludden (Institut National des Sciences de l'Univers) and Jean-Paul Montagner (Direction Générale de la Recherche et de l'Innovation) for their support. The Indonesian Agency for the Assessment and Application of Technology (BPPT) is greatly acknowledged for its help and support during the planning stage of the cruise. The French Hydrographic Service (SHOM) helps to validate swath-bathymetric data. Bernard Ollivier (IPEV) and his technical team are particularly acknowledged for their dedicated work at sea. We thank Bob Engdahl for providing his relocated teleseismic events in the Sumatra region. We thank Jo Curray, Jamie Austin and an anonymous reviewer for their careful and constructive reviews. Financial supports were provided by the Agence Nationale de la Recherche (ANR), the Délégation Inter-ministérielle pour le Tsunami (DIPT), Ifremer and IPEV.

Legend of figures

Figure 1: a) Seismicity in the Sumatra-Andaman region relocated and color classified by depth from 1918 through 25 December 2004 {Engdahl, 2007 #514}. The size of hypocenters is function of the magnitude Mb. The two focal mechanisms in black correspond to the Sumatra and Nias events. Bathymetry and topography in gray {Sandwell, 1994 #121}. The red line with triangles is the trench location and red lines are tectonic features from Hsu and Sibuet {, 2005 #519}. Co-seismic slip contours every 5 m in purple from Chlieh et al. {, 2007 #515} show different geographic distributions in the Nicobar and Sumatra sectors roughly separated by a dashed green line. b) Aftershock seismicity between the dates of the Sumatra and Nias events. Legend as in Fig. 1a. c) Focal mechanisms from the Harvard catalog color classified by depth from 1964 through 25 December 2004. Beach balls in lower hemisphere projection are plotted at the location of the relocated earthquakes of Engdahl et al. {, 2007 #514}. Legend as in Fig. 1a. d) Aftershocks focal mechanisms from the Harvard catalog color classified by depth from 25 December 2004 through 28 March 2005.

Figure 2: Swath-bathymetric data collected along a 370x75 km stripe located southeast of the India-Indonesia water limit over the regional bathymetry {Sandwell, 1994 #121}. Light from the southwest. Main structural elements in red. Lines with triangles are thrust faults. Thick continuous red lines with triangles are potential splay faults determined from swath-bathymetric and 3.5 kHz data. The solid N-S trending blue lines are the locations of N-S fracture zones of the Wharton Basin and their associated N-S trending valleys in the wedge.

Figure 3: Detailed structural interpretation of the upper part of the accretionary wedge located southwest of the Outer Arc. Blue grayish lines, N-S trending valleys of the wedge; thick continuous red lines with triangles, thrust faults as in Fig. 2. Light from the southwest.

Figure 4: 3.5 kHz Profile A located in Fig. 3 across a popup feature and small elongated tilted basins observed within a piggy-back basin.

Figure 5: 3.5 kHz Profile B located in Fig. 3 across the same piggy-back basin than Fig. 4 with numerous seaward vergence thrust faults showing signs of recent tectonic activity.

Figure 6: Detailed structural interpretation close to the deformation front. Blue grayish lines, N-S trending valleys of the wedge; thick continuous red lines with triangles, thrust faults as in Fig. 2. Light from the southwest.

Figure 7: Block diagrams of a) the toe of the accretionary wedge, with a minor landslide located close to the trench and the Major Thrust Fault located at the base of the eroded wall (festoon); b) the main part of the wedge with the well-imaged N-S valleys linked to N-S fracture zone features of the lower plate.

Figure 8: 3.5 kHz Profile C located in Figs. 3 and 6 across a N-S oriented fold with a possible E-W compressive component.

Figure 9: 3.5 kHz Profile D located in Figs. 3 and 6 across potential N-S left lateral strike slips.

Figure 10: a) Aftershock determinations from the two Japanese and French networks of seismometers. In blue, aftershocks determined during 10 days of the recording period (20 February - 13 March 2005) by Araki et al. {, 2006 #496} using 17 seismometers (triangles). In red, 665 aftershocks determined from our survey using 20 seismometers (stars) from 22 July 2005 to 3 August 2005. Magnitudes of earthquakes scaled in the upper left part of the figure. Large solid and dashed lines with triangles are post-seismic active splay faults (Lower and Median Splay Faults) and non-active post-seismic features, respectively. Thick blue lines are the N-S fracture zones and their prolongation below the lower part of the wedge. Note the presence of a swarm of 186 events located at the northern extremity of the 93.2°E fracture zone and of a large number of events along the northern extremity of the 93.6°E fracture zone, highlighting the shift of seismicity along the Median Splay Fault from S-E of it in February 2005 to N-W of it in August 2005. The projected synthetic profile 2 shows in purple the slab and active splay faults determined from the hypocenters distribution. b) Seismicity along Profile 2 in function of the distance to the trench. Only hypocenters located inside the Japanese {Araki, 2006 #496} and French (498 events) networks are shown in blue and red, respectively. In purple, slab and splay faults deduced from the distribution of hypocenters. Note the presence of lower plate events in the 40-60 km and 90-130 km stripes, suggesting the re-activation of lower plate fracture zones.

Figure 11: Sketch of co- and post-seismic motions of the Great Sumatra-Andaman Earthquake. a) Topographic cross-section along Profile 1 located in Figure 10a. Identified active and inactive splay faults corresponding to those of Figure 10 in continuous and dashed black lines, respectively. MT, Major Thrust; LSF, Lower Splay Fault; MSF, Median Splay Fault; USF, Upper Splay Fault. b) Same cross-section without vertical exaggeration with co-seismic motion along the slab and the Upper Splay Fault in purple. Inactive splay faults and features in thin black lines. c) In purple, post-seismic motion along the slab and the Lower and Median Splay Faults determined from the distribution of aftershocks without vertical exaggeration. Inactive splay faults and features in thin black lines. d) Sketch of potential shear-type ruptures along the West-Andaman or Sumatra Faults, which might give rise to destructive earthquake damages in the future.

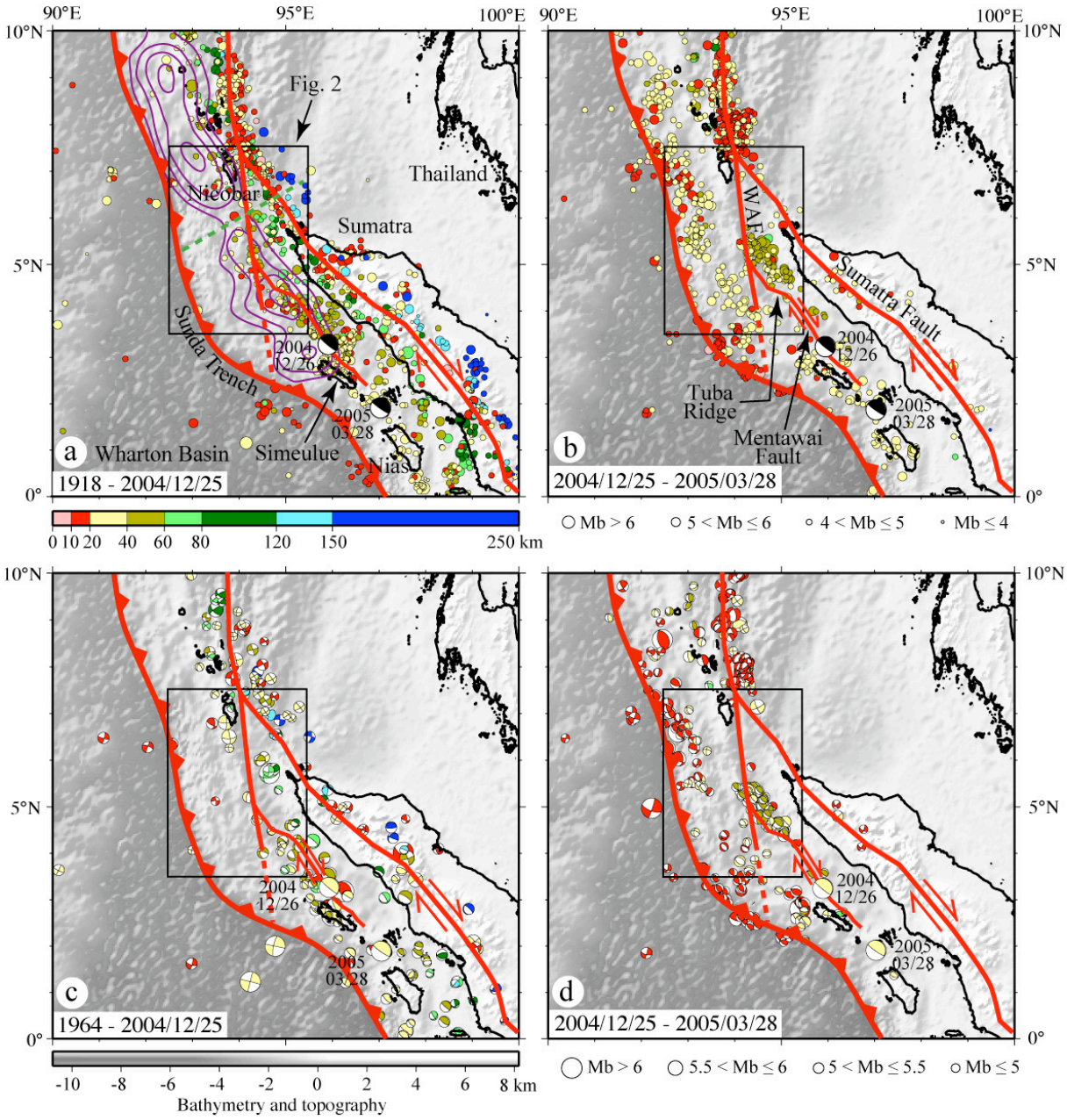

Sibuet et al., Figure 1

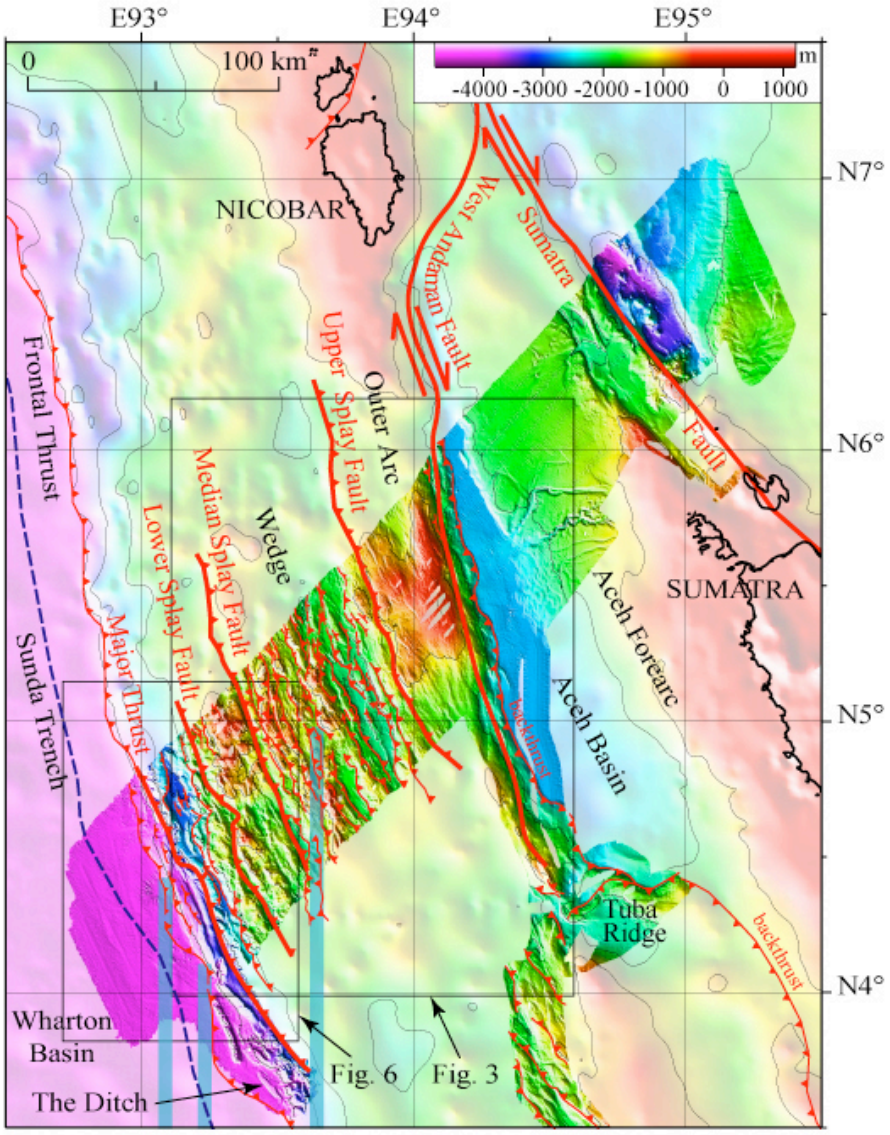

Sibuet et al., Figure 2

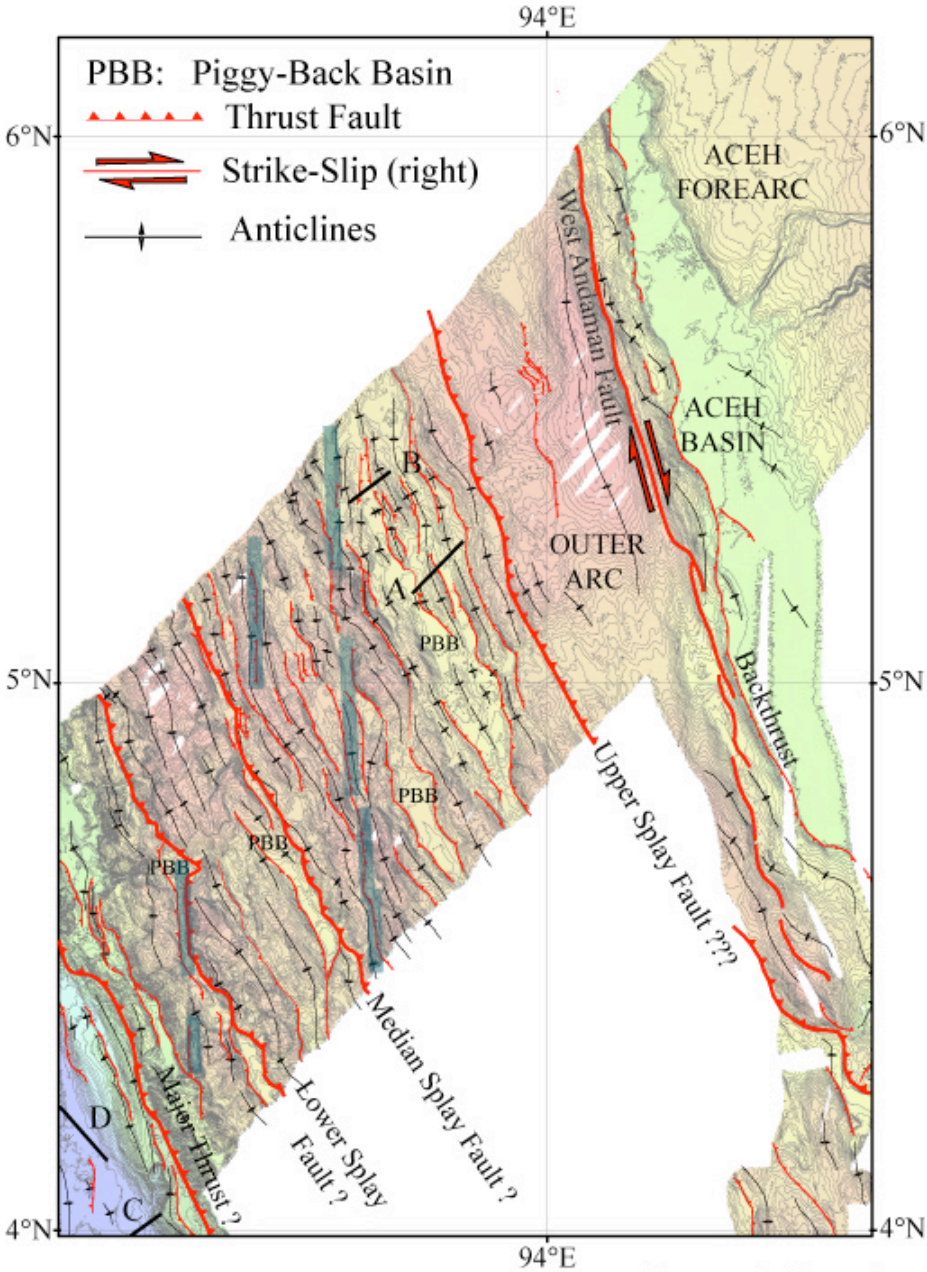

Sibuet et al., Figure 3

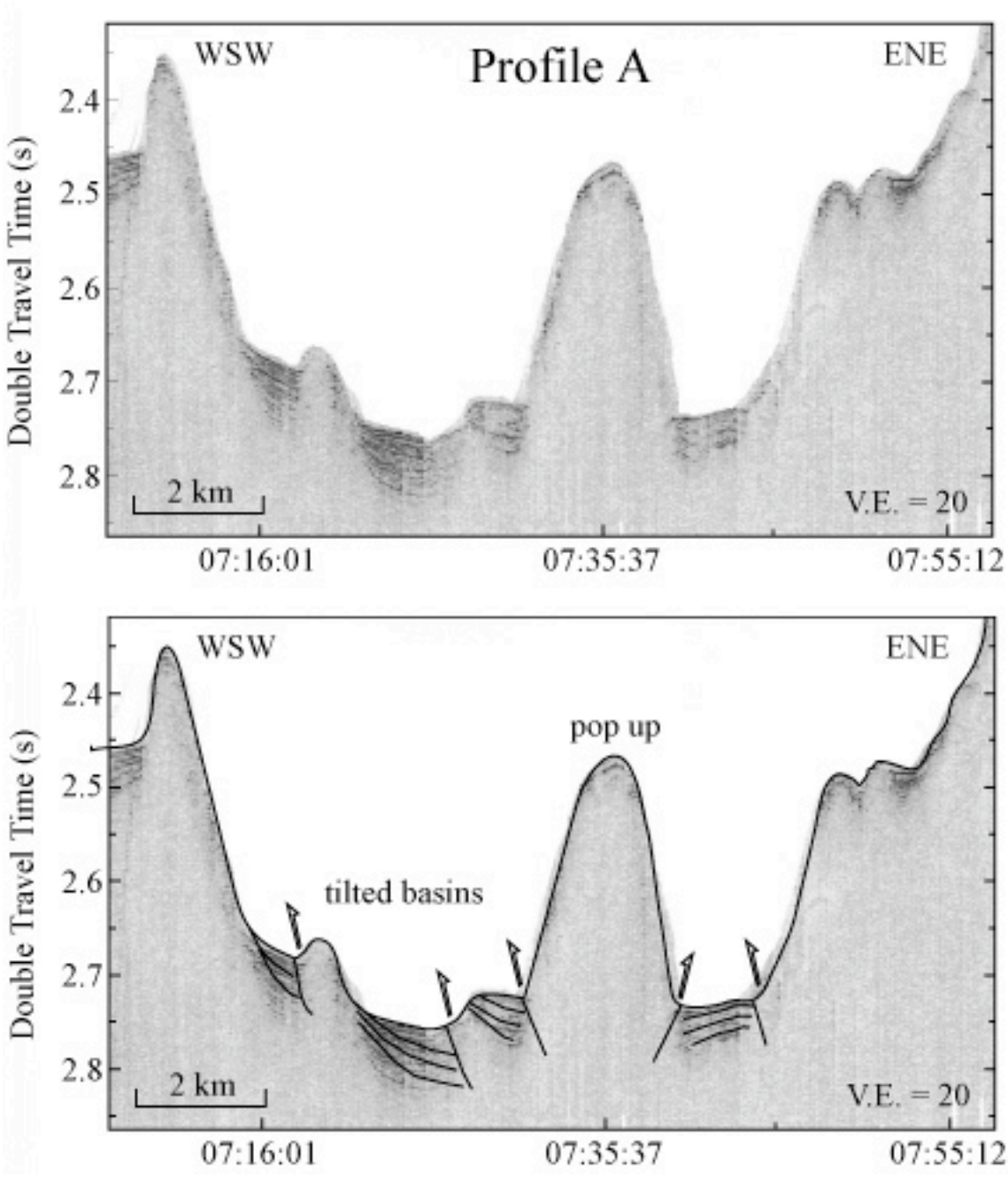

Sibuet et al., Figure 4

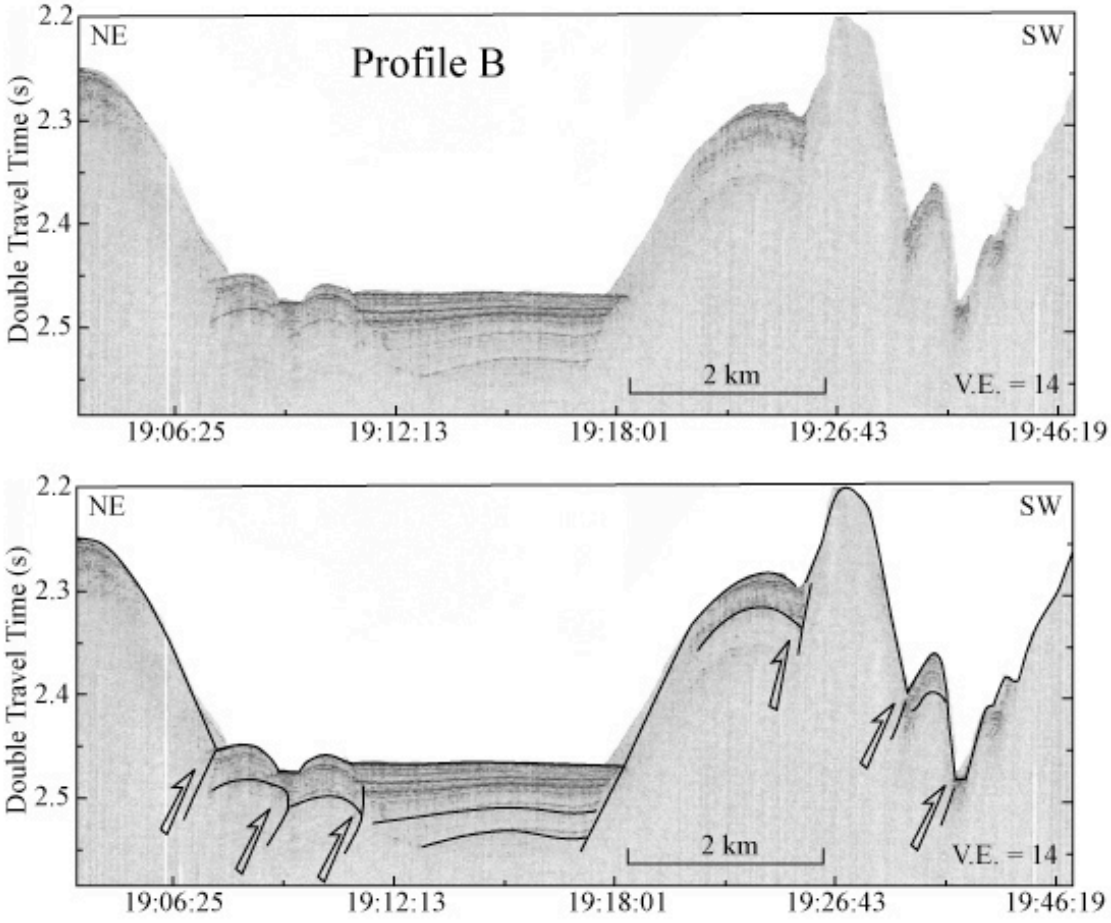

Sibuet et al., Figure 5

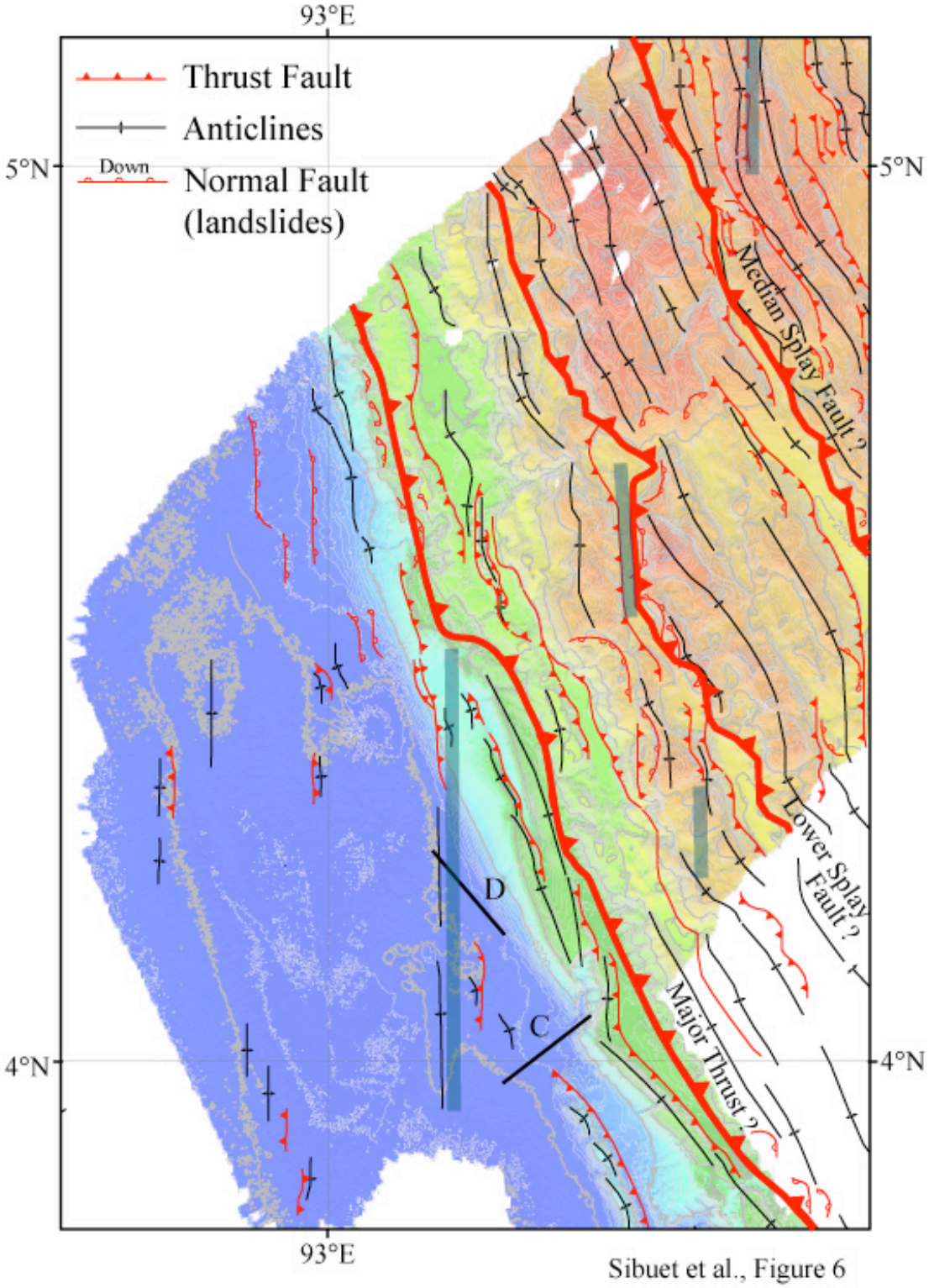

Sibuet et al., Figure 6

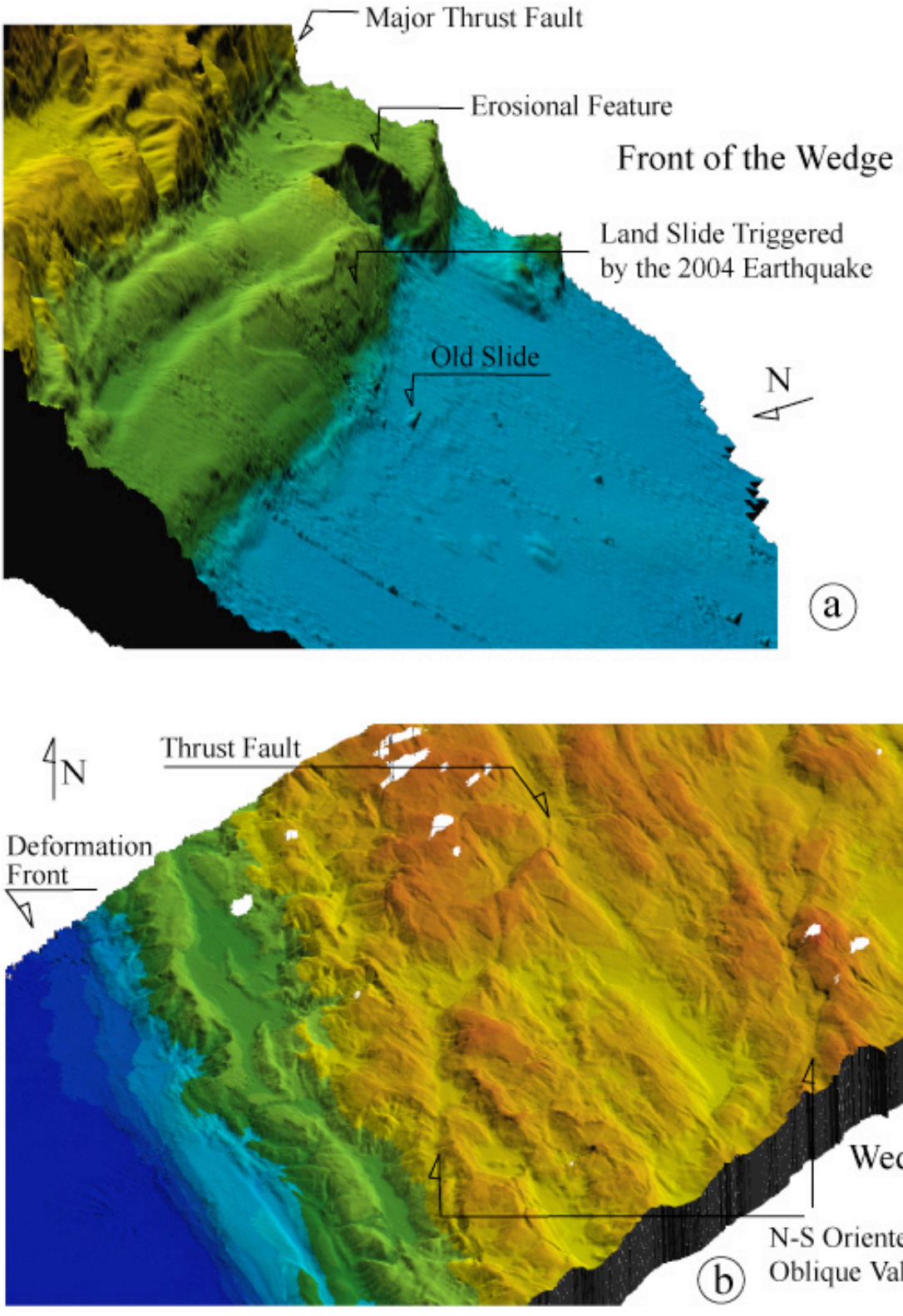

Sibuet et al., Figure 7

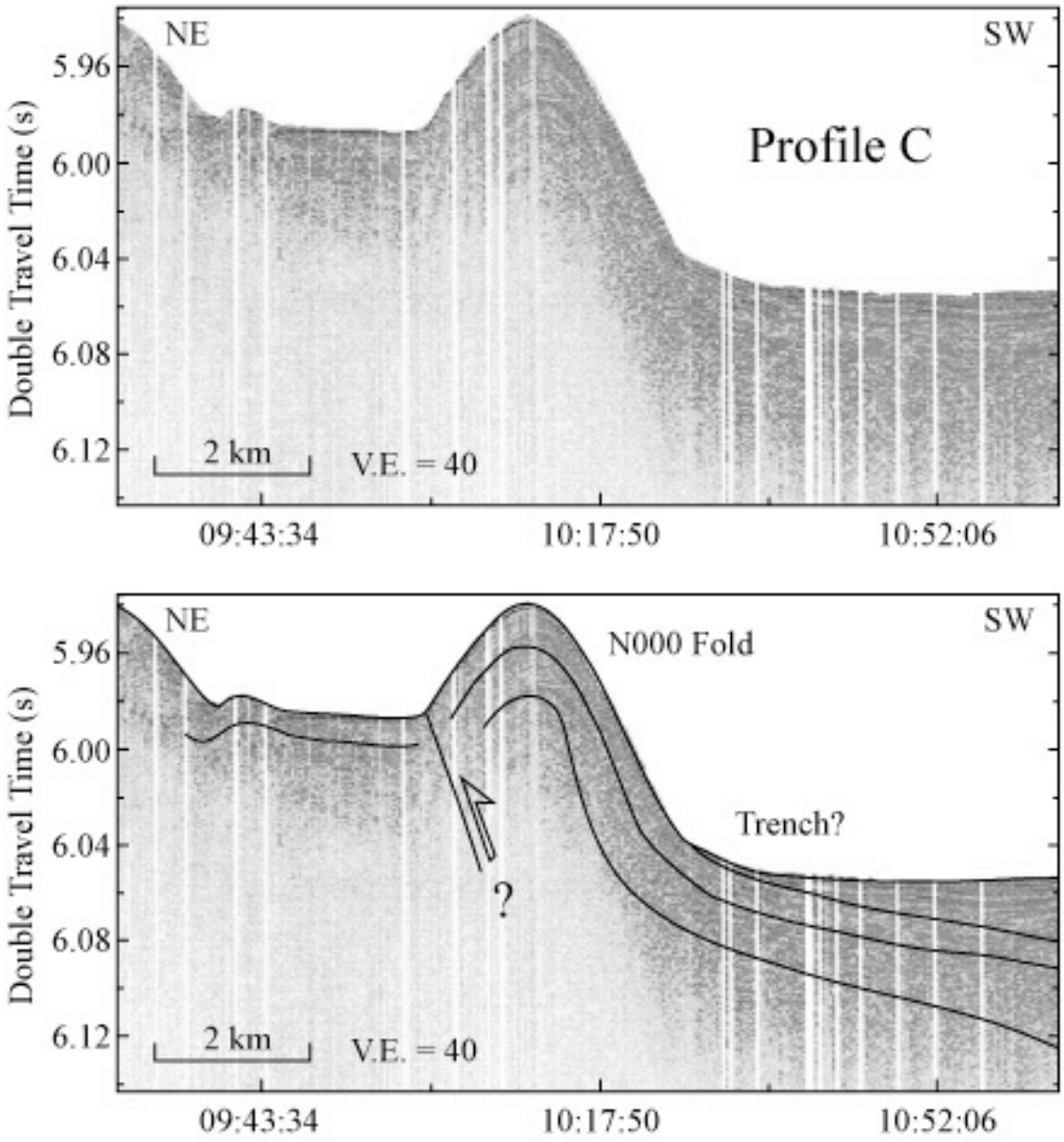

Sibuet et al., Figure 8

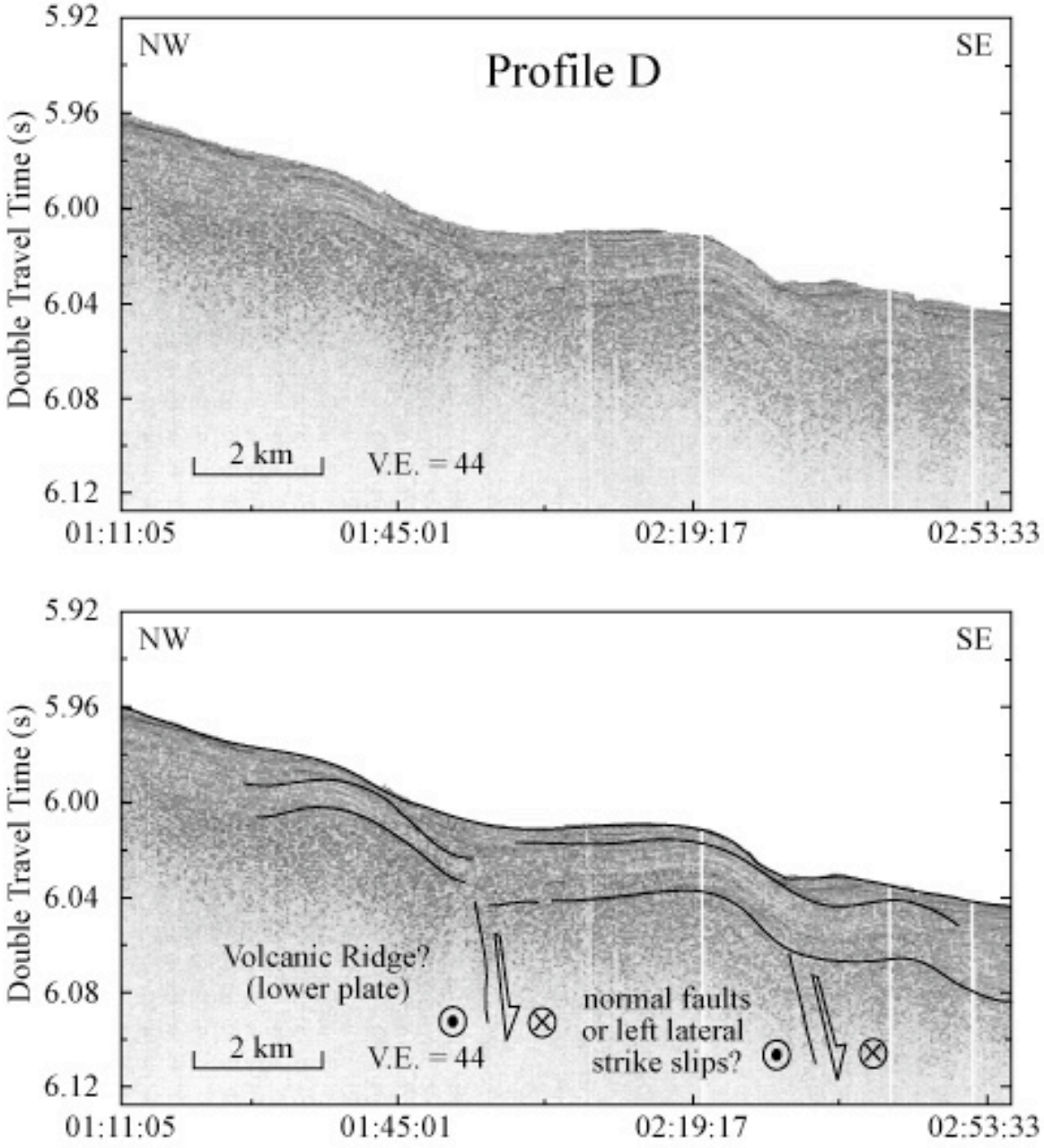

Sibuet et al., Figure 9

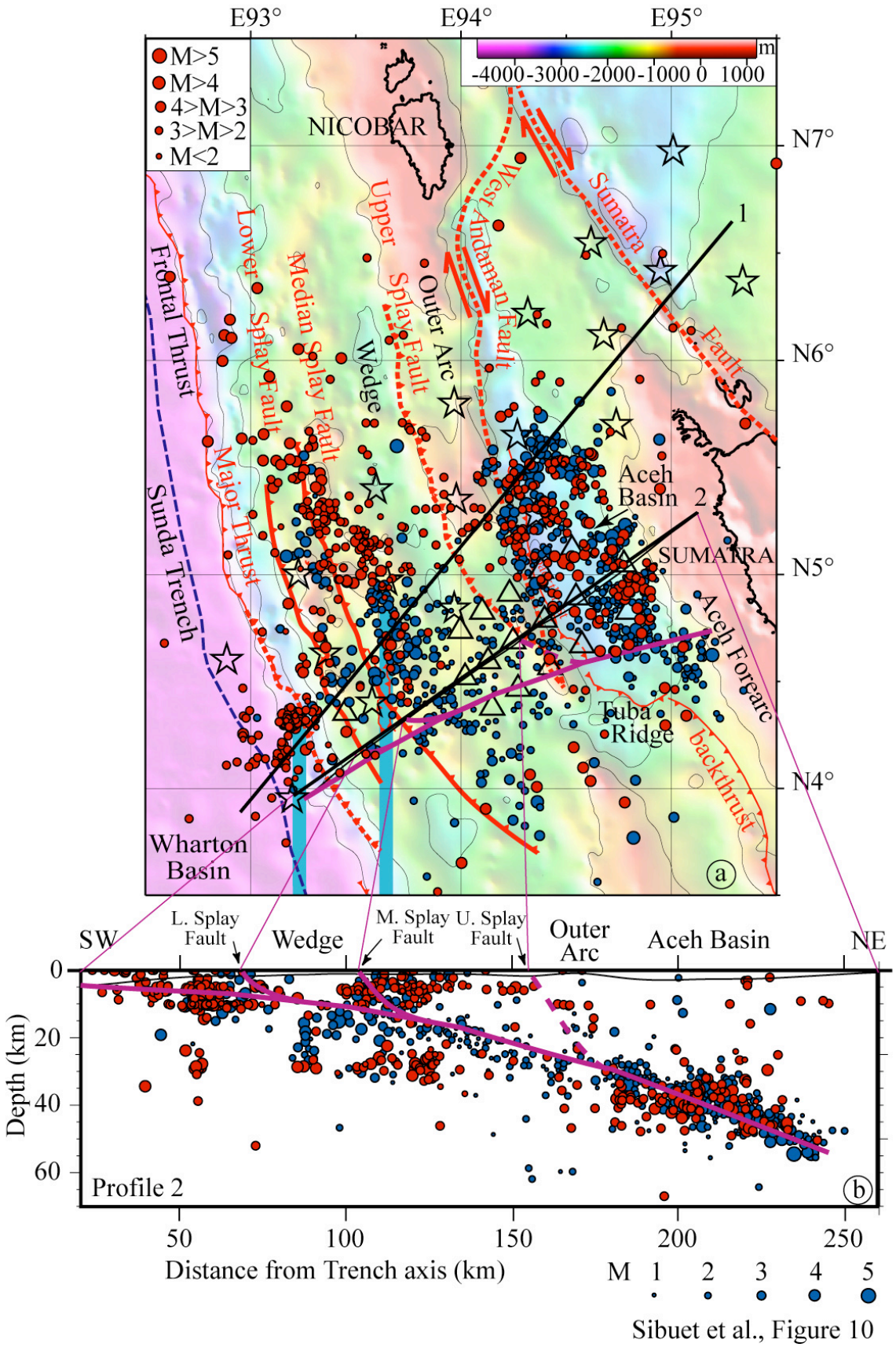

Sibuet et al., Figure 10

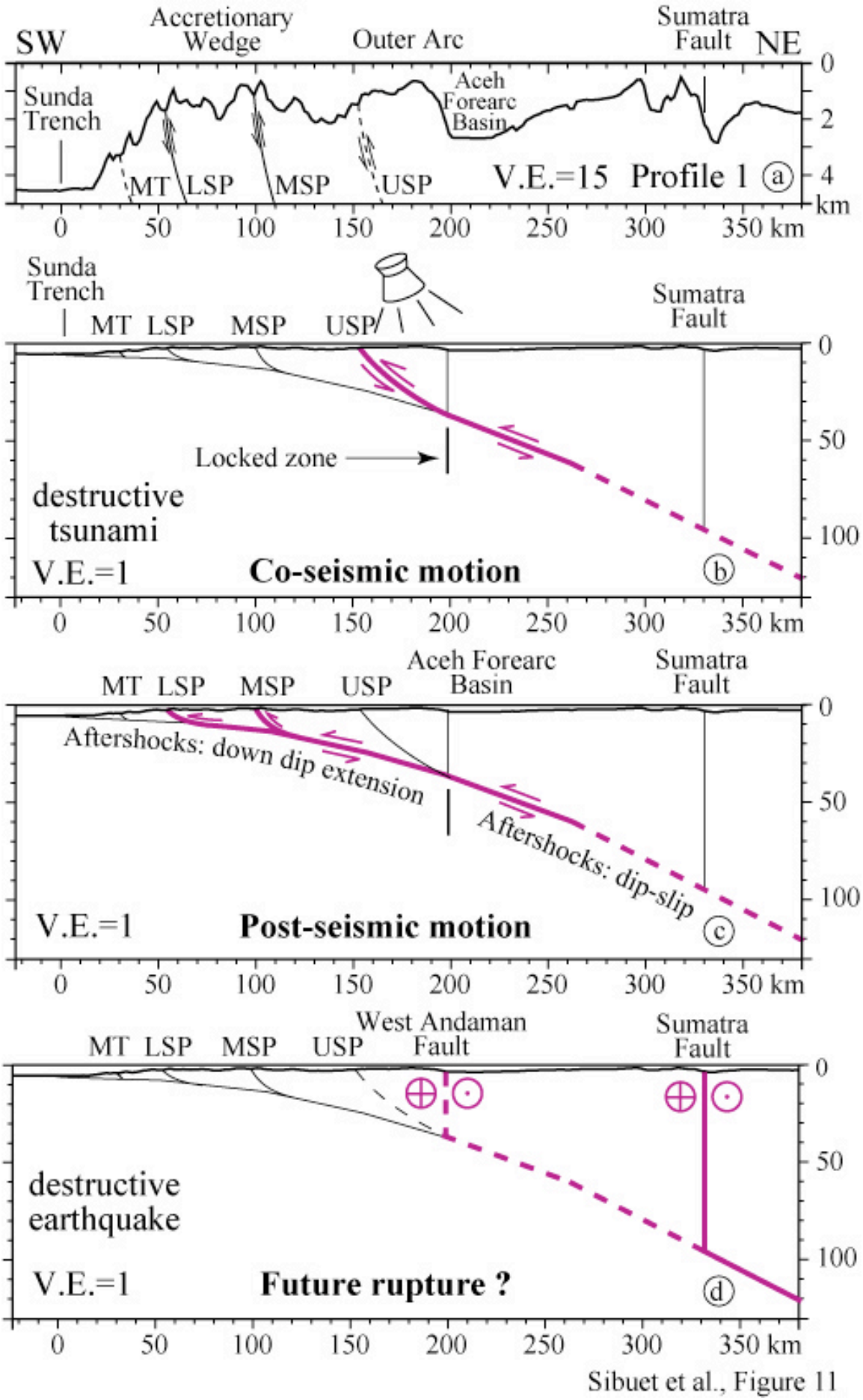

Sibuet et al., Figure 11